materials

MDPI

Article

Effect of Activating Agent on the Properties of TiO_2/Activated Carbon Heterostructures for Solar Photocatalytic Degradation of Acetaminophen

Manuel Peñas-Garzón *, Almudena Gómez-Avilés, Jorge Bedia, Juan J. Rodriguez and Carolina Belver

Departamento de Ingeniería Química, Facultad de Ciencias, Universidad Autónoma de Madrid, Campus Cantoblanco, E-28049 Madrid, Spain; almudena.gomeza@uam.es (A.G.-A.); jorge.bedia@uam.es (J.B.); juanjo.rodriguez@uam.es (J.J.R.); carolina.belver@uam.es (C.B.)

* Correspondence: manuel.pennas@uam.es; Tel.: +34-91-497-35-98

Received: 12 December 2018; Accepted: 23 January 2019; Published: 25 January 2019

Abstract: Several activated carbons (ACs) were prepared by chemical activation of lignin with different activating agents ($FeCl_3$, $ZnCl_2$, H_3PO_4 and KOH) and used for synthesizing TiO_2/activated carbon heterostructures. These heterostructures were obtained by the combination of the activated carbons with a titania precursor using a solvothermal treatment. The synthesized materials were fully characterized (Wavelength-dispersive X-ray fluorescence (WDXRF), X-ray diffraction (XRD), Scanning electron microscopy (SEM), N2 adsorption-desorption, Fourier transform infrared (FTIR) and UV-visible diffuse reflectance spectra (UV-Vis DRS) and further used in the photodegradation of a target pharmaceutical compound (acetaminophen). All heterostructures were composed of anatase phase regardless of the activated carbon used, while the porous texture and surface chemistry depended on the chemical compound used to activate the lignin. Among all heterostructures studied, that obtained by $FeCl_3$-activation yielded complete conversion of acetaminophen after 6 h of reaction under solar-simulated irradiation, also showing high conversion after successive cycles. Although the reaction rate was lower than the observed with bare TiO_2, the heterostructure showed higher settling velocity, thus being considerably easier to recover from the reaction medium.

Keywords: Lignin; activating agent; TiO_2/activated carbon; heterostructures; solar photocatalysis; water purification; acetaminophen

1. Introduction

In recent decades, the treatment of contaminants of emerging concern in water effluents, such as pharmaceuticals and personal care products (PPCPs), is receiving special attention because of their commonly recalcitrant and toxic character [1–3]. Those species enter to water bodies through industrial discharges but also from municipal wastewaters [4,5]. In wastewater treatment plants (WWTPs), organic matter and suspended solids can be efficiently removed, but most PPCPs are highly resistant to conventional biological treatments, such as the activated sludge. In this context, there is a growing demand for technologies that can deal with these emerging contaminants in cost-effective terms. Advanced oxidation processes (AOPs), which include Fenton-based, UV- and sunlight-assisted, ozonation or heterogeneous catalytic systems, among others, have been so far widely investigated technologies for that purpose [6–8]. Heterogeneous photocatalysis offers the advantage of operating at mild conditions and the opportunity of using solar light as a sustainable and cost-effective energy source, which is a main challenge regarding the economy of this potential solution. In heterogeneous photocatalysis, the irradiation of a semiconductor induces the generation of charges (electrons, e^- and

holes, h^+) that, on the surface of the solid, promote the formation of highly oxidizing species, such as hydroxyl ($HO^\bullet$) or superoxide ($O_2^{\bullet -}$) radicals. The energy absorbed by the semiconductor has to be enough to overcome its band gap energy (E_g), i.e., the energy barrier between the valence and the conduction bands of the material [9]. Titanium dioxide, TiO_2, is the most used semiconductor among the wide variety of photocatalysts investigated for the treatment of water. It presents the advantages of high photochemical activity and stability, low-toxicity and affordable costs. However, commercial TiO_2 powder has quite limited adsorption capacity, due to its low surface area, besides its difficult recovery from the reaction medium because of its small particle size, within the nanometric scale [10].

Combining TiO_2 with carbonaceous materials can be a useful approach to overcome those drawbacks. Carbonaceous materials mainly include activated carbon, carbon fibers or nanotubes and graphene. Among them, activated carbons (ACs) have the lowest cost [11,12]. ACs are amorphous carbonaceous solids with high and well-developed porosity, with surface areas from 500 to 3,000 $m^2 \cdot g-^1$, in the whole range of micro- (<2 nm), meso- (2–50 nm) and macropores (>50 nm). Biomass materials, including residues such as agricultural, forestry and associated industrial wastes, can be used as precursors, thus providing valorization opportunities. This is the case of lignin, a high C-content natural biopolymer which is one of the main constituents of lignocellulosic materials, in particular of wood. Cellulose pulp manufacture leaves huge amounts of modified lignin in the black liquors, which is mostly used as fuel. The future biorefinery is expected to produce also high quantities of lignin [13–15], which will demand the development of valorization approaches.

The activation of a carbon precursor can be achieved through two main well-known ways: i) physical activation, consisting most commonly in previous pyrolysis of the precursor and subsequent partial gasification of the resulting char with steam or CO_2; and ii) chemical activation, where the carbon precursor is physically mixed with the activating agent and heat-treated in inert atmosphere [16–19]. This second method gives in general higher carbon yield due to the combined processes of dehydration and tars inhibition promoted by the activating agent. The activating agents are transition metal salts (e.g., $FeCl_3$ or $ZnCl_2$), acids (as H_3PO_4 or H_2SO_4) and alkaline bases (such as KOH or NaOH) [20–23], playing an important role on the development of different porous textures [24]. The mass ratio between the carbonaceous precursor and the activating agent is also considered a determining variable in that respect [16,18]. The chemical agent also has a very significant effect on the surface chemistry of the resulting activated carbons.

The use of TiO_2/activated carbon heterostructures for the photocatalytic treatment of PPCPs has been investigated in the last decade. Awfa et al. [11] have recently reported a critical review on this topic. Ultrapure water solutions with high concentrations of pollutants (from 10 to 150 $mg \cdot L^{-1}$) have been tested under simulated sunlight and visible light. Almost complete depletion of the PPCPs was achieved, but in most cases adsorption and photodegradation processes were combined due to the low adsorption times followed in the dark. In this work, different TiO_2/activated carbon heterostructures were synthesized by solvothermal treatment using a titanium alkoxide as a titania precursor and an activated carbon from chemical activation of lignin with different agents (namely, $FeCl_3$, $ZnCl_2$, KOH and H_3PO_4). The resulting materials were fully characterized and tested in the photodegradation of a pharmaceutical compound (acetaminophen). The novelty of this work is focused on the comparative use of different activating agents to obtain several activated carbons that will be used for preparing TiO_2/activated carbon heterostructures, with the aim to obtain novel photocatalysts for the degradation of a contaminant of emerging concern. Special attention was paid to achieve adsorption equilibrium prior to the photocatalytic test, evaluating all heterostructures at similar initial concentration of the target compound and equal TiO_2 content in each experiment under simulated solar light. Finally, the separation of the photocatalyst by settling and its performance and stability after recycles were checked.

2. Materials and Methods

2.1. Materials

Lignin (from LignoTech Ibérica S.A., Cantabria, Spain) was selected as the carbon precursor for activated carbons. $FeCl_3 \cdot 6H_2O$ (≥97%), $ZnCl_2$ (97%), H_3PO_4 (85%) and KOH (85%), used as agents for the chemical activation of lignin, were all purchased from Panreac (Panreac Química S.L.U., Barcelona, Spain). Titanium tetrabutoxide ($Ti(OBu)_4$; ≥97%) was supplied by Sigma Aldrich (Sigma-Aldrich Co., St. Louis, MO, USA). Ethanol (EtOH; 96%) was obtained from Panreac (Panreac Química S.L.U., Barcelona, Spain). HCl (≥37%) and NaOH (≥95%) were purchased from Sigma Aldrich (Sigma-Aldrich Co., St. Louis, MO, USA) and Scharlau (Scharlab S.L., Barcelona, Spain), respectively. Acetaminophen (ACE; ≥99%, from Sigma-Aldrich Co., St. Louis, MO, USA) was selected as the target emerging contaminant. Acetonitrile (HPLC grade, Scharlau, Scharlab S.L., Barcelona, Spain) and acetic acid (≥99%, Sigma Aldrich Sigma-Aldrich Co., St. Louis, MO, USA) were used as the mobile phase for liquid chromatography. Ultrapure water (Type I, 18.2 MΩ·cm) and deionized water (Type II) were used in this work.

2.2. Synthesis of TiO_2/AC Heterostructures

2.2.1. Preparation of Activated Carbons

Activated carbons were obtained by chemical activation of lignin using different activating agents. Table 1 summarizes the activation conditions of the different carbons [20,25–27]. Firstly, 5 g of lignin and the corresponding mass of activating agent were physically mixed. For KOH, the lignin was previously carbonized at 800 °C for 2 h, avoiding the fragmentation and solubilization of the lignin caused by strongly nucleophilic hydroxyl ions from the activating agent [28]. Then, the mixtures were dried at 60 °C overnight and heat-treated at the desired temperature for 2 h under N_2 flow (100 $Ncm^3 \cdot min^{-1}$) in a horizontal stainless-steel tube furnace, using a heating rate of 10 °C $\cdot min^{-1}$. Then, the samples were cooled down to room temperature under N_2 flow. The resulting solids were further washed in two steps. Firstly, with HCl (0.1 M) at 70 °C for 2 h to remove the residual activating agent and secondly, with deionized water at room temperature up to neutral pH. The final materials were dried overnight in an oven at 60 °C. The resulting activated carbons were denoted as Fe-C, Zn-C, P-C and K-C, according to the activating agent used. The activating agent to lignin mass ratio was established in each case after previous experiments where different values were tested.

Table 1. Activation conditions of the different carbons.

Sample	Activating Agent	Act. Agent: Lignin Mass Ratio	Activation Temperature (°C)
Fe-C	$FeCl_3$	3:1	800
Zn-C	$ZnCl_2$	3:1	500
P-C	H_3PO_4	3:1	500
K-C	KOH	4:1	900

2.2.2. Solvothermal Synthesis of TiO_2/Activated Carbon Heterostructures

TiO_2/activated carbon heterostructures were obtained following a solvothermal synthesis [29]. Preliminary trials were conducted where different TiO_2/AC mass ratios were checked prior to select the most suitable to achieve heterostructures based on anatase phase. After these studies, the amount of TiO_2 was fixed at 80% in all cases. Thus, 58 mg of activated carbon were suspended into 45 mL of EtOH at room temperature for 5 min, leading to the solution A. At the same time, 1 mL of $Ti(OBu)_4$ was diluted in 15 mL of EtOH for 5 min (solution B). Then, solution B was added dropwise to solution A under continuous stirring until complete homogenization. A solution of 3 mL of ultrapure water in 15 mL of EtOH was incorporated dropwise to produce the hydrolysis of the Ti precursor. The mixture was stirred for 5 min, transferred to a 125 mL Teflon-lined stainless-steel autoclave, and heated at 160 °C

for 3 h. After the reaction, the solid was separated by centrifugation (5300 rpm, 10 min), washed three times with deionized water and finally with ethanol. The resulting grey materials were dried at 60 °C overnight. The heterostructures were labelled as TiO_2/x-C, namely TiO_2/Fe-C, TiO_2/Zn-C, TiO_2/P-C and TiO_2/K-C, depending on the activated carbon used to form the heterostructure. For comparison, bare TiO_2 was also obtained under the same conditions in the absence of activated carbon.

2.3. Characterization Techniques

A Bruker S8 TIGER spectrometer (Bruker, Billerica, MA, USA) under inert atmosphere (He) (maximum voltage of 60 kV and maximum current of 170 mA) was used to determine the percentage of TiO_2 in the final samples by wavelength-dispersive X-ray fluorescence (WDXRF). X-ray diffraction (XRD) patterns were recorded on a Bruker D8 diffractometer (Bruker, Billerica, MA, USA) with a scintillation detector, using Cu-Kα source, with a scan step of $1^\circ \cdot min^{-1}$ between 5 and 70° of 2θ. Scherrer's equation was used to estimate the average crystal size (D) from the most intense diffraction peak (101) of anatase phase. A Quanta 3D Field Emission Gun (FEG) microscope (FEI Company, Hillsboro, OR, USA) was used to obtain the scanning electron microscopy (SEM) images of the samples. The particles size distributions were obtained from these images by using the ImageJ software (National Institutes of Health, Bethesda, MD, USA). In each case, 20 particles per image (out of a total of five images) were analyzed to achieve a good representation of the particle size.

The porous texture was characterized by N_2 adsorption-desorption at −196 °C using a Micromeritics TriStar 123 static volumetric system (Micromeritics Instrument Corp., Norcross, GA, USA). The samples were previously outgassed under vacuum at 150 °C overnight in a Florprep 060 Micromeritics device (Micromeritics Instrument Corp., Norcross, GA, USA). The specific surface area (S_{BET}) was determined by the Brunauer-Emmett-Teller (BET) method [30], while the external or non-microporous surface area (S_{EXT}) and micropore surface area (S_{MP}) were calculated using the t-plot method [31]. Fourier Transform Infrared (FTIR) spectra (wavenumber range 4000–400 cm^{-1}) were recorded on a Bruker iFS 66VS spectrometer (Bruker, Billerica, MA, USA) using a resolution of 2 cm^{-1}. Samples were previously prepared using KBr pellets. The pH drift method [32] was used to determine the pH at the point of zero charge (pH_{pzc}). Briefly, 50 cm^3 of 0.01 M NaCl solution at initial pH (adjusted between 3–11 using 0.1 M HCl or NaOH) were placed in a closed titration vessel. Then, 20 mg of the sample were suspended and nitrogen was bubbled before starting the test in order to stabilize the initial pH by removing dissolved gasses. The final pH, measured after 5 h, was plotted versus the initial one. The pH_{pzc} is given by value where the curve crosses $pH_{initial} = pH_{final}$.

A Shimadzu 2501PC UV-vis spectrophotometer (Shimadzu Corporation, Kyoto, Japan) was used to record UV-vis diffuse reflectance spectra (UV-vis DRS) in the 250–800 nm region using $BaSO_4$ as reference material. The band gap values were estimated using the Tauc Plot standard technique [33]. Considering that all heterostructures are indirect semiconductors, as TiO_2 [34], this method uses the equation $\alpha h\nu = \alpha \cdot (h\nu - E_g)^{1/2}$, where α, h, ν and E_g are the absorption coefficient, Planck constant, light frequency and the energy gap of the semiconductor, respectively. Plotting $(\alpha h\upsilon)^{1/2}$ vs. $h\upsilon$ results in a curve with a linear region. The extrapolation of this linear branch to the X-axis provides the band gap value of the material.

2.4. Photocatalytic Tests

The photocatalytic degradation of acetaminophen (ACE) was performed in a 500 mL Pyrex jacketed reactor (Segainvex UAM, Madrid, Spain) at a controlled temperature of 25 °C. The experiments were carried out inside a Suntest solar simulator (Suntest XLS+, ATLAS, Mount Prospect, IL, USA) equipped with a 765–250 $W \cdot m^{-2}$ Xe lamp. Solar radiation was simulated using a "Daylight" filter (cuts off $\lambda \leq 290$ nm), selecting 600 $W \cdot m^{-2}$ (107.14 klx) as irradiation intensity. In each test, the concentration of photocatalyst was set so that all the experiments were performed with the same amount of TiO_2, 250 $mg \cdot L^{-1}$. For this purpose, the results obtained after characterization by WDXRF were used to know the amount of TiO_2 of each sample. The calculated amount of photocatalyst was

dispersed in 150 mL deionized aqueous solution containing the contaminant. Prior to the photocatalytic tests, the adsorption capacity of each heterostructure was estimated since the heterostructures showed very different porous textures. Hereby, each catalyst was contacted with ACE solutions of different concentrations, measuring the amount adsorbed at equilibrium after 16 h. That value was used to adjust the initial concentration of ACE for each catalyst, which was in all cases 5 $mg \cdot L^{-1}$. Further, the suspension was exposed to simulated solar light for 6 h. Samples of 450 µL were collected at different times and filtered using PTFE syringeless filters (Scharlau, Scharlab S.L., Barcelona, Spain) (Whatman 0.2 µm). The liquid phase was analyzed by HPLC (Shimadzu Prominence-I LC-2030C, Shimadzu Corporation, Kyoto, Japan) equipped with a diode array detector (SPD-M30A) and a reverse phase C18 column (Eclipse Plus 5 µm, Agilent Technologies, Santa Clara, CA, USA) to measure the ACE concentration (detection wavelength set at 246 nm). A mixture of acetonitrile/acetic acid 0.1% *v/v* (gradient method: 10/90–40/60% (0–17 min)) was used as the mobile phase, with a constant flow of 0.7 $mL \cdot min^{-1}$. Total organic carbon (TOC) was measured at the beginning and end of the reaction using a Shimadzu TOC-L analyzer (Shimadzu Corporation, Kyoto, Japan). The experiments were carried out in duplicate. Settling tests were performed with catalysts suspensions of 1 $g \cdot L^{-1}$. The settling profiles versus time were recorded using a Shimadzu 2501PC UV-vis spectrophotometer (Shimadzu Corporation, Kyoto, Japan) (double beam), measuring the absorbance at 600 nm (in which the extinction of light is mainly due to the scattering caused by the particles of the suspension). In these tests, 4 mL of the suspension were placed in a quartz cuvette and the absorbance were recorded continuously for 2 h. Deionized water in absence of the catalyst was used as blank. In parallel, 100 mL of the catalysts suspensions with the same concentration were placed in graduated cylinders allowing the natural sedimentation of the particles. Pictures at different time intervals were taken for comparison.

3. Results and Discussion

3.1. Characterization of TiO_2/Activated Carbon Heterostructures

The XRD diffractograms of the TiO_2/x-C heterostructures synthesized are depicted in Figure 1 together with that of the TiO_2 prepared as reference. All the samples show the characteristic peaks of the anatase phase (JCPDS file No. 78-2486), whose (hkl) planes are marked in the Figure 1. No peaks assigned to other crystal phases of TiO_2 (e.g., rutile and brookite) or other from the AC were detected. That was also the situation with TiO_2/C heterostructures synthesized by a similar procedure using glucose as carbon precursor [29]. Thus, solvothermal synthesis at 160 °C allowed the development of the crystalline structure of titania without the need of further heat treatment. Comparing the diffractograms, the most intense peak of anatase (101) differs in width depending of the samples. Usually, the widening of the diffraction peaks is associated with the reduction of the crystal size and the creation of defects in the crystalline structure. The anatase crystal size (D) was calculated by using the Scherrer's equation and the position and width of the (101) peak. The values are collected in Table 2. The bare TiO_2 prepared by this solvothermal treatment exhibits a small crystal size, lower than that reported for anatase TiO_2 prepared by other methods [35]. In the TiO_2/x-C samples, even smaller TiO_2 crystal sizes are observed, the values depending on the nature of the activating agent used to prepare the AC. The lowest anatase crystal size was obtained with Zn-C. These values are analogous to those reported for other TiO_2/AC hybrids prepared by the sol-gel method that required a calcination step in air [36,37]. The amount of TiO_2 incorporated in the heterostructures was determined by WDXRF and the results are included in Table 2. Most of the samples have a TiO_2 content similar to the expected (80%), with only the sample TiO_2/Zn-C showing some significant deviation. Additional samples were prepared by decreasing the percentage of TiO_2, but the results obtained in terms of photocatalytic activity for ACE degradation were considerably poorer and thus, those samples were discarded.

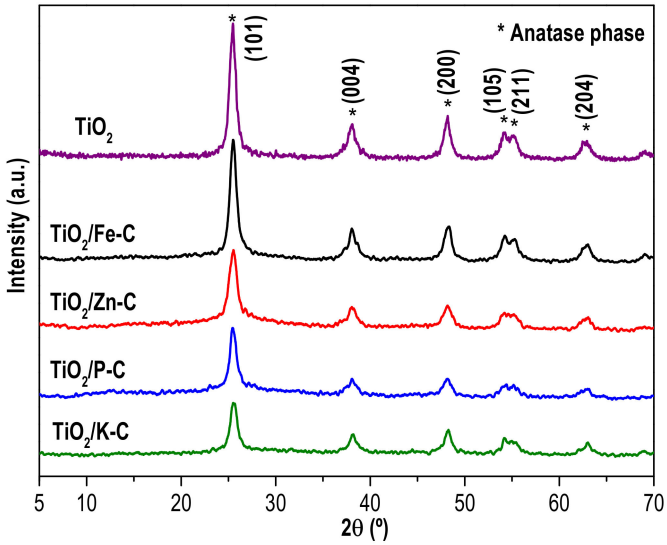

Figure 1. XRD patterns of the TiO_2/activated carbon heterostructures and bare TiO_2. Characteristic peaks of anatase phase (JCPDS-78–2486) are indicated (*).

Table 2. TiO_2 content, average crystal size (D), band gap (E_g) and pH_{pzc} of the heterostructures.

Sample	%TiO_2 [a]	D (nm) [b]	E_g (eV)	pH_{pzc} [c]
TiO_2/Fe-C	75.9	10.1	3.28	6.36
TiO_2/Zn-C	68.5	8.6	3.42	5.96
TiO_2/P-C	81.3	10.6	3.50	4.86
TiO_2/K-C	83.9	9.4	3.45	6.17
TiO_2	n.m	10.5	3.33	6.58

[a] Determined by WDXRF (n.m. not measured). [b] Average crystal size from (101) diffraction peak. [c] Determined from the drift method.

All synthesized heterostructures showed an external spherical-like morphology, as it can be observed from the SEM images (Figure 2), analogous to the bare TiO_2. Figure 2 also includes the histograms of the particle size distribution, obtained by measuring ca. to 100 particles for each sample. The average diameter of TiO_2 particles is higher than the obtained for the heterostructures, which fall within the range of 0.24–0.28 μm. However, the particles of TiO_2/x-C show a higher degree of agglomeration. This suggests that the presence of activated carbon inhibits the growth of the TiO_2 particles, as previously reported by Wang et al. [38]. The size distribution is unimodal in all cases except for TiO_2/Zn-C, which shows a bimodal profile centered at 0.21 and 0.30 μm.

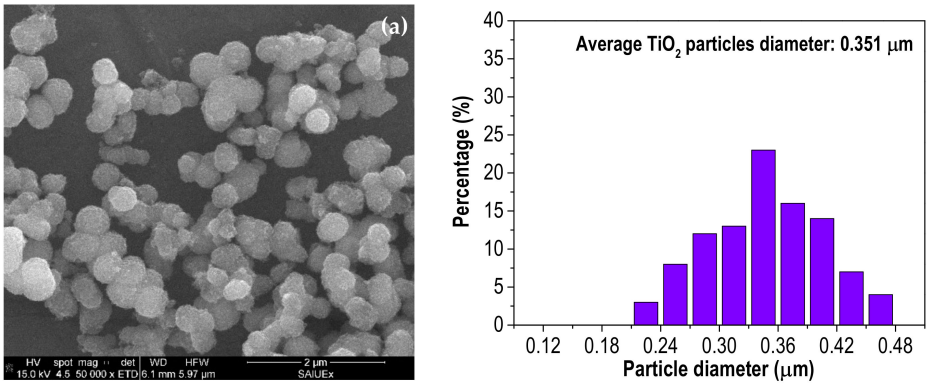

Figure 2. *Cont.*

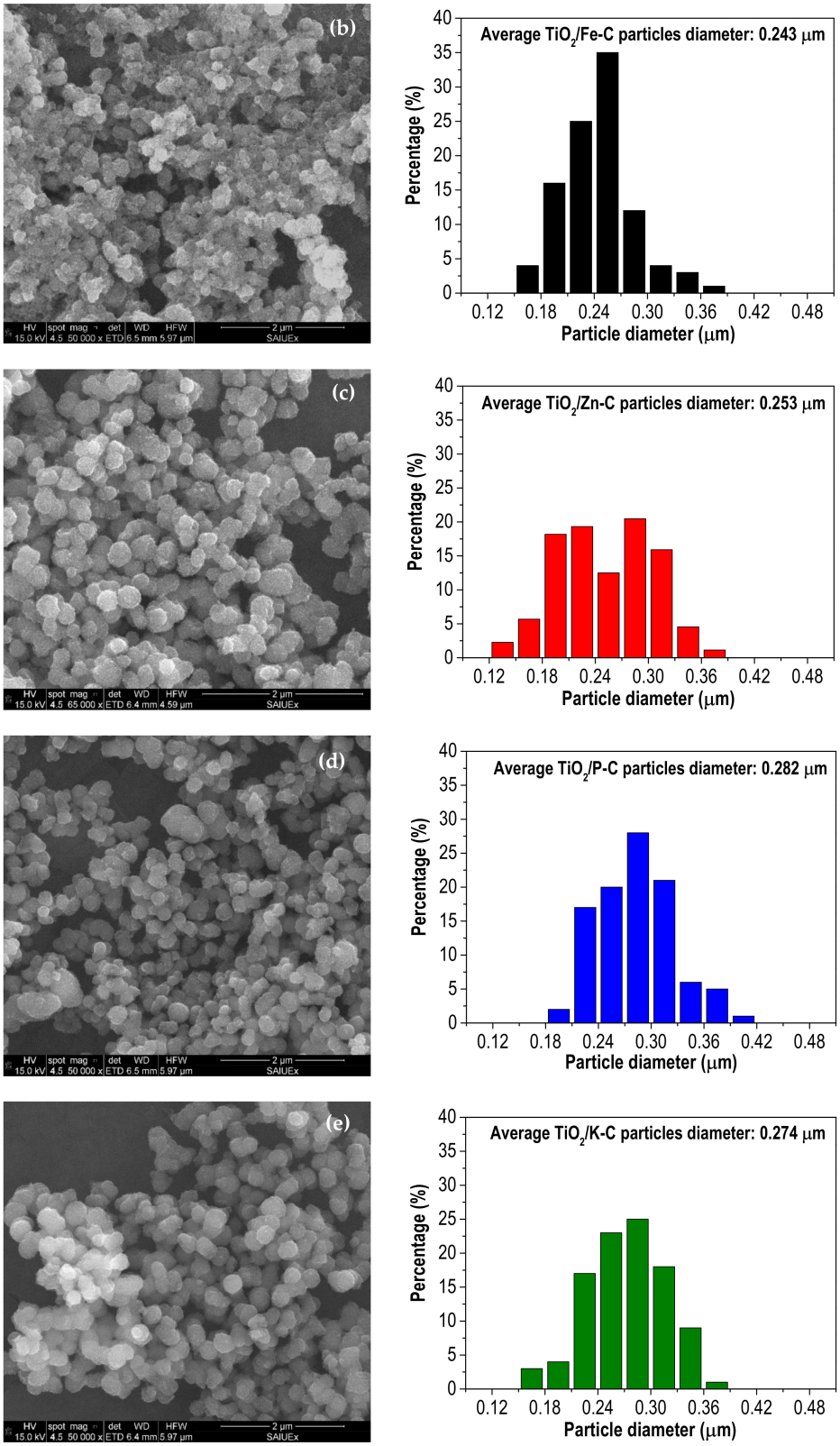

Figure 2. SEM images and particle size distribution of: (**a**) TiO_2; (**b**) TiO_2/Fe-C; (**c**) TiO_2/Zn-C; (**d**) TiO_2/P-C; (**e**) TiO_2/K-C.

Nitrogen adsorption–desorption isotherms of activated carbons and TiO_2/x-C heterostructures are represented in Figure 3. K-C and Fe-C ACs (Figure 3a) show typical type I isotherms, characteristic

of microporous materials, according to the IUPAC classification [39]. In both cases, the major uptake occurs at low relative pressures followed by an almost horizontal branch, this shape being indicative of highly microporous solids. In contrast, Zn-C and P-C describe hybrid I/II type isotherms with hysteresis loops at $P/P_0 > 0.4$, suggesting the existence of a well-developed microporous structure but with significant contribution of mesoporosity. Figure 3b shows that the different TiO_2/x-C heterostructures present type II isotherms, with a remarkable decrease of adsorption, indicating that the porous structure of the activated carbons has been partially blocked by the incorporation of TiO_2.

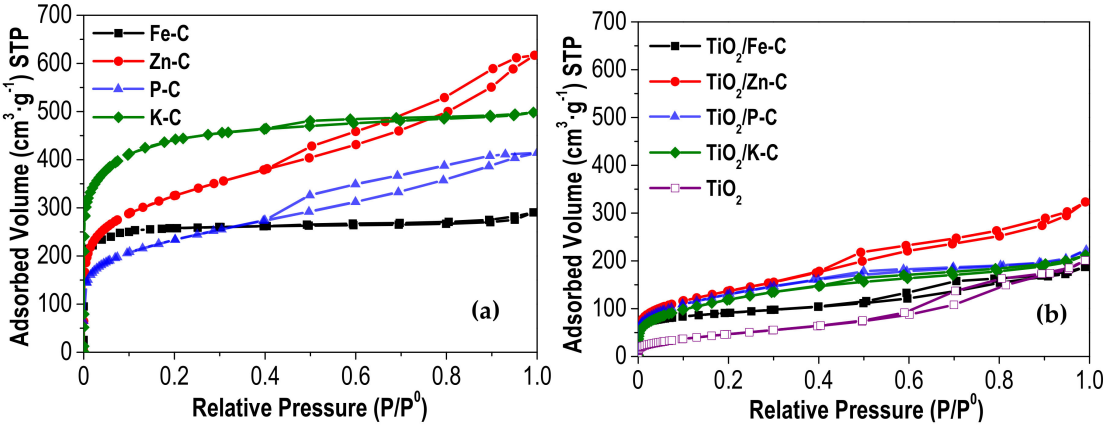

Figure 3. N_2 adsorption-desorption isotherms (−196 °C) of (**a**) activated carbons and (**b**) TiO_2 and TiO_2/x-C heterostructures.

Table 3 summarizes the surface area values (BET, microporous and external or non-microporous) characterizing the porous texture of the synthesized materials. The development of surface area depends on the chemical activating agent used, following the order K-C >> Zn-C >> P-C > Fe-C. It should be mentioned the high development of mesoporosity upon $ZnCl_2$-activation (as showed by the high value of the so-called external surface area). According to literature [28,40,41], the chemical activation mechanisms consist in the oxidation and/or dehydration of the precursor, including complex different reactions depending on the agent. However, a general mechanism involved in this type of activation is still not very clear. The dehydration during the heat treatment of the lignin seems to be the most determinant effect in the chemical activation with $ZnCl_2$ and H_3PO_4. In the case of H_3PO_4, a strong Brønsted acid, it yields a partial depolymerization, followed by dehydration and condensation processes; whereas in the case of $ZnCl_2$, a Lewis acid, the reaction with lignin is proton-catalyzed producing the dehydration and further aromatization of the carbon skeleton [42]. KOH reacts with the solid precursor by means of redox reactions, resulting in the microporosity development after oxidizing carbon to CO and CO_2. This predominant formation of micropores has also been observed with $FeCl_3$-activation, in contrast to $ZnCl_2$, ascribing a similar behavior to that of alkali agents [20]. In the case of TiO_2, the entire surface area corresponds to mesopores. Further introduction of activated carbon in the solvothermal synthesis step allowed obtaining heterostructures including microporosity.

The surface functional groups of all activated carbons and synthesized heterostructures were assessed from the FTIR spectra (Figure 4). The activated carbons (Figure 4a) show the characteristic bands due to the presence of adsorbed water, appearing the –OH stretching and bending bands at 3400 and 1600 cm^{-1}, respectively [29,43,44]. In the K-C carbon, the peaks located at 1537 and 1408 cm^{-1} were assigned to the stretching of –C=C in the skeletal aromatic ring and –CO stretching of carbonate groups, respectively [43,45,46]. Stretching of –COC can be observed in the absorption bands centered in the range of 1170–1030 cm^{-1}. This vibration can be produced from diverse oxygenated groups, thus varying the main absorption peak [29,43]. In P-C, the weak bands centered at 1060 and 980 cm^{-1} can be attributed to –PO and –POC groups. TiO_2 and TiO_2/x-C FTIR spectra (Figure 4b), are very similar among them, indicating the homogeneous distribution of TiO_2 over the heterostructure. There are three main absorption bands. Those centered at 3400 and 1625 cm^{-1} are associated with

adsorbed water, as previously indicated for activated carbons. The wide band located between 800 and 400 cm^{-1} corresponds to the characteristic –Ti-O-Ti stretching band of TiO_2 [47,48]. This band appears in all samples, with a maximum ca. to 700 cm^{-1}, which corroborates the generation of titania phase in all the heterostructures. The high intensity and width of this band overlaps those characteristic bands described for the activated carbons, taking into account that the TiO_2 percentage of these heterostructures is fairly high (ca. 80%). In the case of TiO_2/P–C, around 1030 cm^{-1} appears a weak shoulder that can be ascribed to the stretching bands of –PO and –POC groups previously described for the corresponding activated carbon.

Table 3. Surface area values of the synthesized materials.

Sample	S_{BET} ($m^2 \cdot g^{-1}$)	S_{MP} ($m^2 \cdot g^{-1}$)	S_{EXT} ($m^2 \cdot g^{-1}$)
Carbonized lignin	62	62	-
Fe-C	756	695	61
Zn-C	1129	451	678
P-C	807	303	504
K-C	1446	1142	304
TiO_2/Fe-C	300	125	175
TiO_2/Zn-C	491	108	383
TiO_2/P-C	435	109	326
TiO_2/K-C	465	156	309
TiO_2	178	-	178

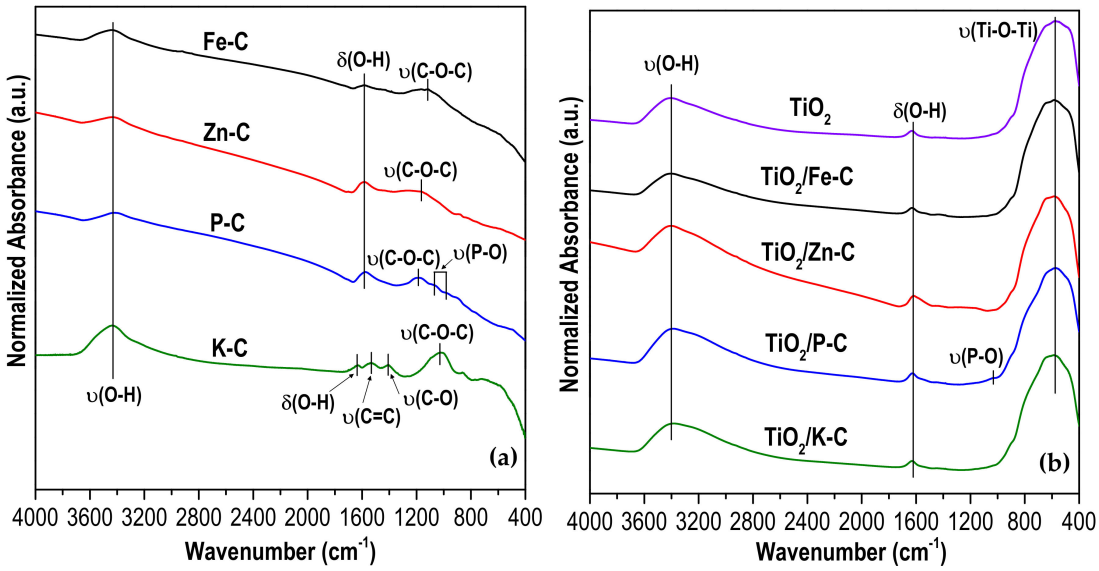

Figure 4. FTIR spectra of: (**a**) activated carbons; (**b**) TiO_2 and TiO_2/x-C heterostructures.

An important parameter regarding the acid-base behavior of the samples is the pH_{pzc}. When the pH of the solution is lower than the pH_{pzc}, the surface of the solid is positively charged, whereas it is negatively charged at pH above the pH_{pzc} of the sample. Table 2 summarizes the pH_{pzc} values of the synthesized heterostructures. The pH_{pzc} of bare TiO_2 is almost neutral, which means that its surface is not charged in neutral water [49,50]. In the case of the heterostructures, it is clear that the pH_{pzc} values depend on the activating agent used during the preparation of the activated carbon, corresponding the lowest value to TiO_2/P-C. The low acidity of $FeCl_3$ (a weak Lewis acid) can result in the introduction of poor acidic groups in the heterostructure surface, giving a pH_{pzc} analogous to that of TiO_2, while the use of H_3PO_4 (a strong Brønsted acid) yields a heterostructure with a low pH_{pzc} probably due to the presence of phosphates that leave OH groups on the surface [17]. Regarding to TiO_2/K-C, despite the basic character of KOH, the solid has a relatively neutral PZC (even lower than that prepared with

$FeCl_3$). This may be due to the fact that after activation the solid was washed with HCl to remove the remaining KOH, thus eliminating the basic sites in the final solid.

The light absorption in the UV and visible region of the synthesized photocatalysts was investigated by UV-vis DRS technique, the resulting spectra are shown in Figure 5a. The absorption band observed in the UV range (below 360 nm) is very similar in all cases, typical of TiO_2. In the visible region, the spectra of the heterostructures do not fall to zero because of their grey color. The effect is more evident in TiO_2/Fe-C and TiO_2/Zn-C, because these samples have lower percentages of TiO_2 (Table 2), yielding the color change from light-to-dark grey. As mentioned above, the band gap values were determined from the UV-vis DRS spectra (according to the Tauc plot method, Figure 5b) and are included in Table 2. The values are fairly similar to that of TiO_2 [51,52], only somewhat higher except in the case of TiO_2/Fe-C. Although it has been reported that the combination of TiO_2 with carbonaceous supports can produce a significant red-shifted displacement of absorption edge, in our heterostructures this has not been observed. This may be due to a more limited interaction between TiO_2 and AC compared to other carbon supports, like graphene or carbon nanotubes [11,12].

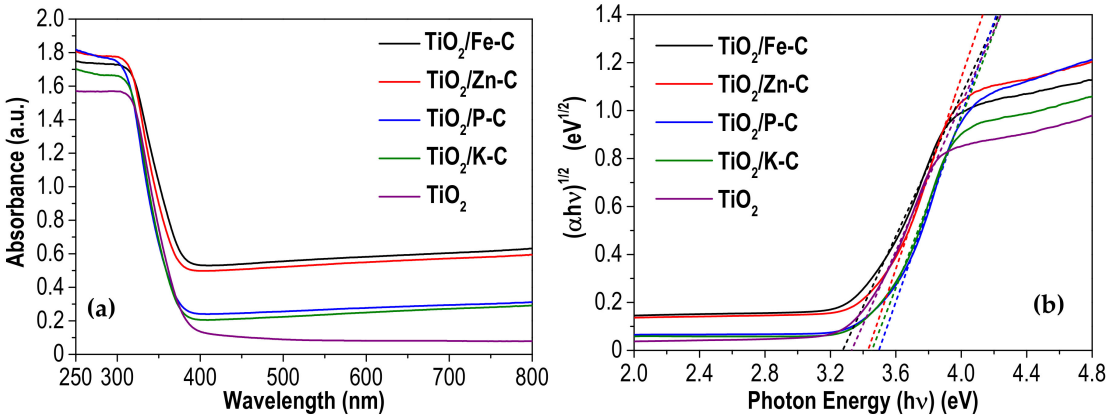

Figure 5. (**a**) UV–vis diffuse absorbance spectra and (**b**) the $(\alpha h\upsilon)^{1/2}$ versus ($h\upsilon$) plot of the synthesized photocatalysts.

3.2. Photocatalytic Tests

The photocatalytic performance of the synthesized heterostructures in the degradation of acetaminophen (ACE) under solar light is depicted in Figure 6, which includes the results with bare TiO_2 for the sake of comparison, as well as a blank experiment, showing the complete stability of ACE under solar light irradiation in absence of catalyst. A comparative study using TiO_2/Fe-C as photocatalyst was also carried out for 6 h with and without simulated solar radiation (Figure S1) after the adsorption period, showing no variation in the ACE concentration in absence of light. As depicted in Figure 6, the light-assisted tests were preceded by a 16-h step in dark to allow the adsorption equilibrium. The differences in the adsorbed quantity of ACE can be explained by means of multiple interactions, such as electrostatic forces or the porous texture. Negligible ACE is adsorbed on the TiO_2 surface, probably due to its low porous development. In contrast, the interaction between the heterostructures and the contaminant seems to be more influenced by electrostatic interactions. The reaction was carried out at an initial pH of 6.9. Due to that the pKa of ACE is 9.9, the molecules of the contaminant are neutrally charged [53]. In contrast, pH_{pzc} of the different heterostructures is below than the reaction pH and, thus, the surface of these photocatalysts is partially negatively charged (increasing the negative charge with decreasing the pH_{pzc}). As a consequence, the quantity of adsorbed ACE decreases as pH_{pzc} diminishes because of partial repulsive electrostatic forces between the neutral molecule and the negative character of the surface of the heterostructures. For example, TiO_2/P-C has the lower pH_{pzc} value of synthesized heterostructures (4.86) and show the lowest adsorption of ACE.

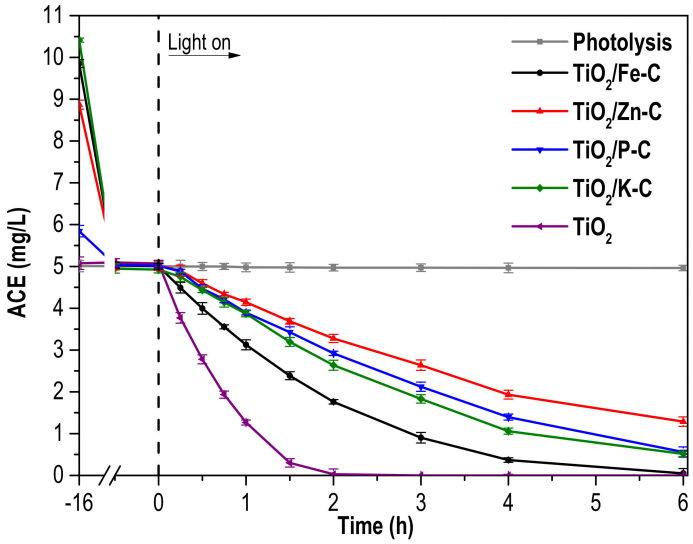

Figure 6. Acetaminophen (ACE) concentration versus time under solar irradiation with TiO_2 and TiO_2/x-C heterostructures ([Photocatalyst]$_0$: 250 mg·L^{-1} of TiO_2; [ACE]$_0$ after adsorption equilibrium: 5 mg·L^{-1}; intensity of irradiation: 600 W·m^{-2}).

It can also be seen in Figure 6 that bare TiO_2 exhibits better photocatalytic performance than the synthesized TiO_2/x-C heterostructures, which is consistent with the easier accessibility of TiO_2 [11], but also with the higher opacity of the suspension caused by the black-grey color. Furthermore, the higher concentration of the heterostructures contributes to their poorer behavior (all the tests were performed with the same amount of TiO_2, and therefore, the amount of solid in the suspension is higher with the TiO_2/x-C heterostructures). Regarding the photocatalytic performance of the synthesized heterostructures, TiO_2/Fe-C appears as the most active, allowing complete ACE conversion after 6 h of reaction, probably due to the lowest band gap of this photocatalyst. The reduction of the photocatalytic activity of TiO_2/activated carbon heterostructures with respect to bare TiO_2 has been previously reported [54,55]. However, other publications claimed the opposite behavior, where the highest photocatalytic activity was found for TiO_2/activated carbon materials [29,56,57]. In some of these works, dark-adsorption was extended for no more than 1 h, which was not probably enough for the complete adsorption equilibrium. Therefore, when the photocatalytic tests started, a combination between adsorption and photocatalytic reaction was carried out. In this sense, the current work focuses only in the photocatalytic performance of the synthesized heterostructures, after reaching adsorption equilibrium.

Since the degradation pathway is of high interest, the final solution was evaluated by ion-exchange chromatography, founding different small carboxylic acids (acetic, formic and malonic) although their total concentration was really low, below 0.07 mg/L. Following the degradation pathway described in the literature [58,59], the presence of other proposed aromatic compounds was investigated but no one could be elucidated. Mineralization of the target pollutant, i.e., complete conversion into CO_2 and H_2O, was followed by measuring the total organic carbon (TOC) in the solution after the 6 h-irradiation time (Table 4). The TiO_2/x-C heterostructures yielded significantly lower degradation of TOC than the bare TiO_2, being again TiO_2/Fe-C the most effective among them.

Table 4. TOC removal after 6 h of solar irradiation with the photocatalysts tested.

Photocatalyst	Removed TOC (%)
TiO_2/Fe-C	43.3
TiO_2/Zn-C	23.9
TiO_2/P-C	35.5
TiO_2/K-C	30.2
TiO_2	59.4

The potential application of a photocatalyst must consider not only its activity but also the recovery from the reaction medium. Settling tests were conducted at neutral pH with bare TiO_2 and TiO_2/Fe-C and the results demonstrated the significantly easier separation of this last (as depicted in Figure 7), probably due to the higher degree of agglomeration observed by SEM. In addition to this, Figure S2 shows pictures of the settling process for both photocatalysts at different times, in which the highest settling velocity of the TiO_2/Fe-C can also be observed, thus being considerably easier to recover the heterostructure from the medium.

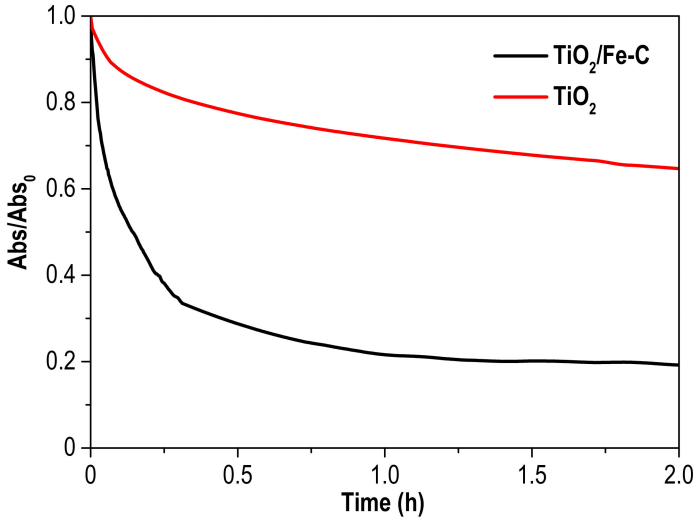

Figure 7. Absorbance evolution profiles (600 nm) during settling test of TiO_2/Fe-C and TiO_2 photocatalysts.

The stability of the photocatalyst with the best recoverability was investigated upon four consecutive cycles. After each cycle, the used TiO_2/Fe-C was filtered, washed with deionized water and dried at 60 °C overnight. Each new cycle was carried out with identical conditions as previously described for the degradation of ACE (Figure 6). As depicted in Figure 8, the heterostructure showed a good performance in the photocatalytic oxidation of ACE after four successive cycles with a slight decrease in the final conversion (92% removal after 6 h of irradiation). The porous texture of the used photocatalyst was also analysed (Figure 9), showing a decrease of the porous network, probably due to the partial blocking of the microporous structure by the adsorbed contaminant or even the oxidized intermediates. Furthermore, the leaching of titania was not detected in the solution after four recycles by using inductive coupled plasma methodology.

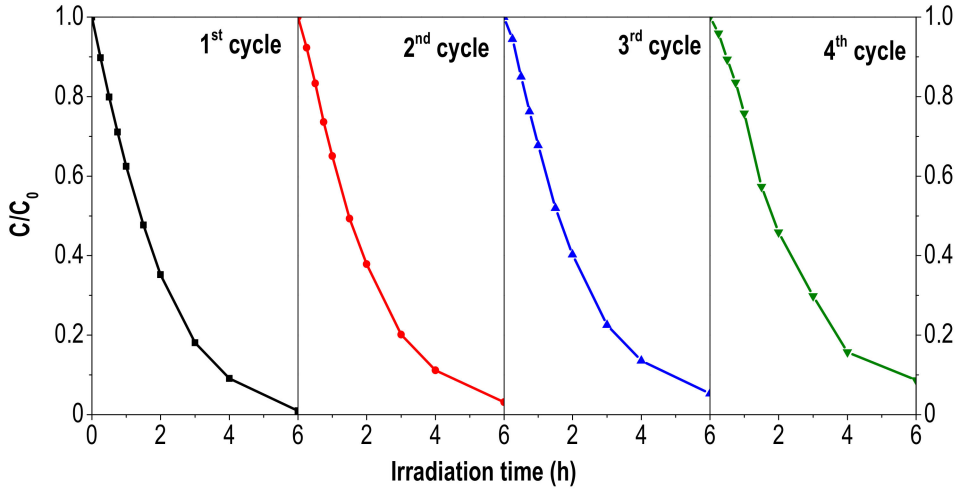

Figure 8. ACE removal with TiO_2/Fe-C during consecutive cycles (Reaction conditions identical than those from Figure 6).

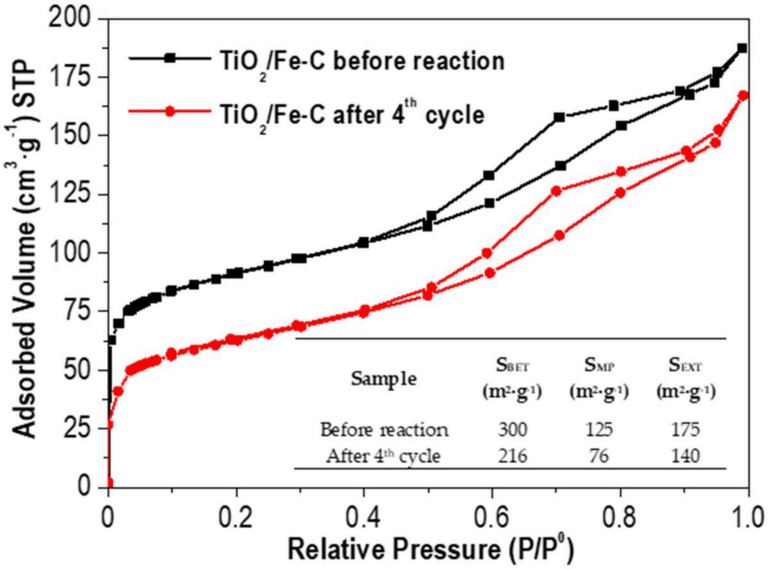

Figure 9. N_2 adsorption-desorption isotherms (−196 °C) of TiO_2/Fe-C before reaction and after four consecutive cycles. Surface area values of the photocatalyst are also included in the embedded table.

4. Conclusions

Solvothermal synthesis of TiO_2/activated carbon (TiO_2/AC) heterostructures was successfully achieved. Lignin has been used as starting material for the ACs following chemical activation with four agents ($FeCl_3$, $ZnCl_2$, H_3PO_4 and KOH). The activated carbons showed a well-developed porous texture and different surface functional oxygenated groups and acid-basic character depending of the activation procedure. XRD patterns of the TiO_2/AC heterostructures confirmed the presence of anatase phase with crystal size close to 10 nm in all cases after the solvothermal synthesis, without the need for further heat-treatment. These materials showed a spherical morphology with a particle size close to 0.27 μm. The presence of activated carbon in the heterostructures increased somewhat the band gap with respect to bare TiO_2, except for TiO_2/Fe-C. TiO_2 and TiO_2/Fe-C showed the best efficiency in the degradation of acetaminophen under solar light, being higher in the case of TiO_2. However, settling experiments demonstrated the easier recovery of the heterostructured material in spite of the lower size of individual particles, because of the higher aggregation observed by SEM. TiO_2/Fe-C also showed a good performance in the photocatalytic oxidation of ACE after four successive cycles.

Supplementary Materials: The following are available online at http://www.mdpi.com/1996-1944/12/3/378/s1, Figure S2: Evolution of ACE concentration with and without irradiation using TiO_2/Fe-C as photocatalyst ([Photocatalyst]$_0$: 250 mg·L^{-1} of TiO_2; [ACE]$_0$ after adsorption equilibrium: 5 mg·L^{-1}; intensity of irradiation: 600 W·m^{-2}); Figure S1: Settling test for TiO_2/Fe-C (left) and TiO_2 (right) samples.

Author Contributions: Conceptualization, J.B., C.B. and J.J.R.; methodology, M.P.-G. and A.G.-A.; writing—original draft preparation, M.P.-G. and A.G.-A.; writing—review and editing, M.P.-G., J.B., C.B. and J.J.R.; supervision, C.B. and J.J.R.; funding acquisition, C.B. and J.J.R.

Funding: This research was funded by the financial support from Spanish MINECO (project CTQ2016-78576-R). M. Peñas-Garzón is indebted to Spanish MECD for FPU16/00576 predoctoral contract.

Acknowledgments: Authors acknowledge Dr. Gamarra and the SAIUEx service for performing the WDXRF and SEM analyses.

Conflicts of Interest: The authors declare no conflict of interest.

References

1. Čelić, M.; Gros, M.; Farré, M.; Barceló, D.; Petrović, M. Pharmaceuticals as chemical markers of wastewater contamination in the vulnerable area of the Ebro Delta (Spain). *Sci. Total Environ.* **2018**, *652*, 952–963. [CrossRef] [PubMed]
2. Yang, Y.; Ok, Y.S.; Kim, K.H.; Kwon, E.E.; Tsang, Y.F. Occurrences and removal of pharmaceuticals and personal care products (PPCPs) in drinking water and water/sewage treatment plants: A review. *Sci. Total Environ.* **2017**, *596–597*, 303–320. [CrossRef] [PubMed]
3. Álvarez-Muñoz, D.; Rodríguez-Mozaz, S.; Maulvault, A.L.; Tediosi, A.; Fernández-Tejedor, M.; Van den Heuvel, F.; Kotterman, M.; Marques, A.; Barceló, D. Occurrence of pharmaceuticals and endocrine disrupting compounds in macroalgaes, bivalves, and fish from coastal areas in Europe. *Environ. Res.* **2015**, *143*, 56–64. [CrossRef] [PubMed]
4. Tran, N.H.; Reinhard, M.; Gin, K.Y.-H. Occurrence and fate of emerging contaminants in municipal wastewater treatment plants from different geographical regions—A review. *Water Res.* **2018**, *133*, 182–207. [CrossRef] [PubMed]
5. Huerta, B.; Rodriguez-Mozaz, S.; Nannou, C.; Nakis, L.; Ruhí, A.; Acuña, V.; Sabater, S.; Barcelo, D. Determination of a broad spectrum of pharmaceuticals and endocrine disruptors in biofilm from a waste water treatment plant-impacted river. *Sci. Total Environ.* **2016**, *540*, 241–249. [CrossRef] [PubMed]
6. Mohapatra, D.P.; Brar, S.K.; Tyagi, R.D.; Picard, P.; Surampalli, R.Y. Analysis and advanced oxidation treatment of a persistent pharmaceutical compound in wastewater and wastewater sludge-carbamazepine. *Sci. Total Environ.* **2014**, *470–471*, 58–75. [CrossRef] [PubMed]
7. Gomes, J.; Costa, R.; Quinta-Ferreira, R.M.; Martins, R.C. Application of ozonation for pharmaceuticals and personal care products removal from water. *Sci. Total Environ.* **2017**, *586*, 265–283. [CrossRef]
8. Xu, Y.; Liu, T.; Zhang, Y.; Ge, F.; Steel, R.M.; Sun, L. Advances in technologies for pharmaceuticals and personal care products removal. *J. Mater. Chem. A* **2017**, *5*, 12001–12014. [CrossRef]
9. Fujishima, A.; Zhang, X.; Tryk, D.A. TiO2 photocatalysis and related surface phenomena. *Surf. Sci. Rep.* **2008**, *63*, 515–582. [CrossRef]
10. Dong, H.; Zeng, G.; Tang, L.; Fan, C.; Zhang, C.; He, X.; He, Y. An overview on limitations of TiO2-based particles for photocatalytic degradation of organic pollutants and the corresponding countermeasures. *Water Res.* **2015**, *79*, 128–146. [CrossRef]
11. Awfa, D.; Ateia, M.; Fujii, M.; Johnson, M.S.; Yoshimura, C. Photodegradation of pharmaceuticals and personal care products in water treatment using carbonaceous-TiO_2 composites: A critical review of recent literature. *Water Res.* **2018**, *142*, 26–45. [PubMed]
12. Leary, R.; Westwood, A. Carbonaceous nanomaterials for the enhancement of TiO_2 photocatalysis. *Carbon* **2011**, *49*, 741–772. [CrossRef]
13. Mosier, N.; Wyman, C.; Dale, B.; Elander, R.; Lee, Y.Y.; Holtzapple, M.; Ladisch, M. Features of promising technologies for pretreatment of lignocellulosic biomass. *Bioresour. Technol.* **2005**, *96*, 673–686. [CrossRef]
14. Alvira, P.; Tomás-Pejó, E.; Ballesteros, M.; Negro, M.J. Pretreatment technologies for an efficient bioethanol production process based on enzymatic hydrolysis: A review. *Bioresour. Technol.* **2010**, *101*, 4851–4861. [CrossRef]

15. Zakzeski, J.; Bruijnincx, P.C.A.; Jongerius, A.L.; Weckhuysen, B.M. The Catalytic Valorization of Lignin for the Production of Renewable Chemicals. *Chem. Rev.* **2010**, *110*, 3552–3599. [PubMed]
16. Rosas, J.M.; Berenguer, R.; Valero-Romero, M.J.; Rodríguez-Mirasol, J.; Cordero, T. Preparation of Different Carbon Materials by Thermochemical Conversion of Lignin. *Front. Mater.* **2014**, *1*, 1–17. [CrossRef]
17. Fernandez-Ruiz, C.; Bedia, J.; Bonal, P.; Rodriguez, J.J.; Gómez-Sainero, L.M. Chloroform conversion into ethane and propane by catalytic hydrodechlorination with Pd supported on activated carbons from lignin. *Catal. Sci. Technol.* **2018**, *8*, 3926–3935. [CrossRef]
18. Rodríguez, J.J.; Cordero, T.; Rodríguez-Mirasol, J. Carbon Materials from Lignin and Their Applications. *Biofuels Biorefineries* **2016**, *6*. [CrossRef]
19. Bouchelta, C.; Medjram, M.S.; Bertrand, O.; Bellat, J.-P. Preparation and characterization of activated carbon from date stones by physical activation with steam. *J. Anal. Appl. Pyrolysis* **2008**, *82*, 70–77. [CrossRef]
20. Bedia, J.; Belver, C.; Ponce, S.; Rodriguez, J.; Rodriguez, J.J. Adsorption of antipyrine by activated carbons from FeCl3-activation of Tara gum. *Chem. Eng. J.* **2018**, *333*, 58–65. [CrossRef]
21. Kumar, A.; Jena, H.M. High surface area microporous activated carbons prepared from Fox nut (Euryale ferox) shell by zinc chloride activation. *Appl. Surf. Sci.* **2015**, *356*, 753–761. [CrossRef]
22. Da Silva Lacerda, V.; López-Sotelo, J.B.; Correa-Guimarães, A.; Hernández-Navarro, S.; Sánchez-Báscones, M.; Navas-Gracia, L.M.; Martín-Ramos, P.; Martín-Gil, J. Rhodamine B removal with activated carbons obtained from lignocellulosic waste. *J. Environ. Manag.* **2015**, *155*, 67–76. [CrossRef] [PubMed]
23. Bedin, K.C.; Martins, A.C.; Cazetta, A.L.; Pezoti, O.; Almeida, V.C. KOH-activated carbon prepared from sucrose spherical carbon: Adsorption equilibrium, kinetic and thermodynamic studies for Methylene Blue removal. *Chem. Eng. J.* **2016**, *286*, 476–484. [CrossRef]
24. Cordero, T.; Duchamp, C.; Chovelon, J.M.; Ferronato, C.; Matos, J. Influence of L-type activated carbons on photocatalytic activity of TiO_2 in 4-chlorophenol photodegradation. *J. Photochem. Photobiol. A Chem.* **2007**, *191*, 122–131. [CrossRef]
25. Gonzalez-Serrano, E.; Cordero, T.; Rodríguez-Mirasol, J.; Rodríguez, J.J. Development of Porosity upon Chemical Activation of Kraft Lignin with $ZnCl_2$. *Ind. Eng. Chem. Res.* **1997**, *36*, 4832–4838. [CrossRef]
26. Bolshtyansky, M.A.; Margaryan, H.L.; Tabiryan, N.V.; Zel'dovich, B.Y. Realization and development of BRIEFING beam reconstruction algorithm and visualization methods. In Proceedings of the Conference on Lasers and Electro-Optics Europe—Technical Digest, San Francisco, CA, USA, 3–8 May 1998; Volume 50, pp. 448–449.
27. Babeł, K.; Jurewicz, K. KOH activated lignin based nanostructured carbon exhibiting high hydrogen electrosorption. *Carbon* **2008**, *46*, 1948–1956. [CrossRef]
28. Marsh, H.; Rodríguez Reinoso, F. *Activated Carbon*; Elsevier: Amsterdam, The Netherlands, 2006; ISBN 9780080455969.
29. Wu, H.; Wu, X.L.; Wang, Z.M.; Aoki, H.; Kutsuna, S.; Jimura, K.; Hayashi, S. Anchoring titanium dioxide on carbon spheres for high-performance visible light photocatalysis. *Appl. Catal. B Environ.* **2017**, *207*, 255–266. [CrossRef]
30. Brunauer, S.; Emmett, P.H.; Teller, E. Adsorption of Gases in Multimolecular Layers. *J. Am. Chem. Soc.* **1938**, *60*, 309–319. [CrossRef]
31. Lippens, B.C.; De Boer, J.H. Studies on pore systems in catalysts: V. The t method. *J. Catal.* **1965**, *4*, 319–323. [CrossRef]
32. Newcombe, G.; Hayes, R.; Drikas, M. Granular activated carbon: Importance of surface properties in the adsorption of naturally occurring organics. *Colloids Surfaces A Physicochem. Eng. Asp.* **1993**, *78*, 65–71. [CrossRef]
33. Tauc, J. Absorption edge and internal electric fields in amorphous semiconductors. *Mater. Res. Bull.* **1970**, *5*, 721–729. [CrossRef]
34. Zhang, J.; Zhou, P.; Liu, J.; Yu, J. New understanding of the difference of photocatalytic activity among anatase, rutile and brookite TiO_2. *Phys. Chem. Chem. Phys.* **2014**, *16*, 20382–20386. [CrossRef] [PubMed]
35. Banerjee, A.N. The design, fabrication, and photocatalytic utility of nanostructured semiconductors: Focus on TiO2-based nanostructures. *Nanotechnol. Sci. Appl.* **2011**, *4*, 35–65. [CrossRef] [PubMed]
36. Liu, S.X.; Chen, X.Y.; Chen, X. A TiO_2/AC composite photocatalyst with high activity and easy separation prepared by a hydrothermal method. *J. Hazard. Mater.* **2007**, *143*, 257–263. [CrossRef] [PubMed]

37. Ouzzine, M.; Romero-Anaya, A.J.; Lillo-Ródenas, M.A.; Linares-Solano, A. Spherical activated carbon as an enhanced support for TiO_2/AC photocatalysts. *Carbon* **2014**, *67*, 104–118. [CrossRef]
38. Wang, X.; Hu, Z.; Chen, Y.; Zhao, G.; Liu, Y.; Wen, Z. A novel approach towards high-performance composite photocatalyst of TiO_2 deposited on activated carbon. *Appl. Surf. Sci.* **2009**, *255*, 3953–3958. [CrossRef]
39. Thommes, M.; Kaneko, K.; Neimark, A.V.; Olivier, J.P.; Rodriguez-Reinoso, F.; Rouquerol, J.; Sing, K.S.W. Physisorption of gases, with special reference to the evaluation of surface area and pore size distribution (IUPAC Technical Report). *Pure Appl. Chem.* **2015**, *87*, 1051–1069. [CrossRef]
40. Lillo-Ródenas, M.; Cazorla-Amorós, D.; Linares-Solano, A. Understanding chemical reactions between carbons and NaOH and KOH. *Carbon* **2003**, *41*, 267–275. [CrossRef]
41. Bedia, J.; Peñas-Garzón, M.; Goméz-Avilés, A.; Rodríguez, J.J.; Belver, C. A Review on Synthesis and Characterization of Biomass-Derived Carbons for Adsorption of Emerging Contaminants from Water. *C* **2018**, *4*, 63. [CrossRef]
42. Caturla, F.; Molina-Sabio, M.; Rodríguez-Reinoso, F. Preparation of activated carbon by chemical activation with $ZnCl_2$. *Carbon* **1991**, *29*, 999–1007. [CrossRef]
43. Shafaee, M.; Goharshadi, E.K.; Mashreghi, M.; Sadeghinia, M. TiO_2 nanoparticles and TiO_2@graphene quantum dots nancomposites as effective visible/solar light photocatalysts. *J. Photochem. Photobiol. A Chem.* **2018**, *357*, 90–102. [CrossRef]
44. Tsai, W.; Chang, C.; Lin, M.; Chien, S.; Sun, H.; Hsieh, M. Adsorption of acid dye onto activated carbons prepared from agricultural waste bagasse by $ZnCl_2$ activation. *Chemosphere* **2001**, *45*, 51–58. [CrossRef]
45. Mohan, D.; Singh, K.P.; Sinha, S.; Gosh, D. Removal of pyridine from aqueous solution using low cost activated carbons derived from agricultural waste materials. *Carbon* **2004**, *42*, 2409–2421. [CrossRef]
46. Deng, H.; Li, G.; Yang, H.; Tang, J.; Tang, J. Preparation of activated carbons from cotton stalk by microwave assisted KOH and K_2CO_3 activation. *Chem. Eng. J.* **2010**, *163*, 373–381. [CrossRef]
47. Zeitler, V.A.; Brown, C.A. The Infrared Spectra of Some Ti-O-Si, Ti-O-Ti and Si-O-Si Compounds. *J. Phys. Chem.* **1957**, *61*, 1174–1177. [CrossRef]
48. Vasconcelos, D.C.L.; Costa, V.C.; Nunes, E.H.M.; Sabioni, A.C.S.; Gasparon, M.; Vasconcelos, W.L. Infrared Spectroscopy of Titania Sol-Gel Coatings on 316L Stainless Steel. *Mater. Sci. Appl.* **2011**, *2*, 1375–1382. [CrossRef]
49. Barroso-Bogeat, A.; Alexandre-Franco, M.; Fernández-González, C.; Macías-García, A.; Gómez-Serrano, V. Preparation of Activated Carbon-SnO_2, TiO_2, and WO_3 Catalysts. Study by FT-IR Spectroscopy. *Ind. Eng. Chem. Res.* **2016**, *55*, 5200–5206. [CrossRef]
50. Bredow, T.; Jug, K. Theoretical investigation of water adsorption at rutile and anatase surfaces. *Surf. Sci.* **1995**, *327*, 398–408. [CrossRef]
51. Khalid, N.R.; Majid, A.; Tahir, M.B.; Niaz, N.A.; Khalid, S. Carbonaceous-TiO_2 nanomaterials for photocatalytic degradation of pollutants: A review. *Ceram. Int.* **2017**, *43*, 14552–14571. [CrossRef]
52. Carp, O.; Huisman, C.L.; Reller, A. Photoinduced reactivity of titanium dioxide. *Prog. Solid State Chem.* **2004**, *32*, 33–177. [CrossRef]
53. Garcia-Ivars, J.; Durá-María, J.; Moscardó-Carreño, C.; Carbonell-Alcaina, C.; Alcaina-Miranda, M.I.; Iborra-Clar, M.I. Rejection of trace pharmaceutically active compounds present in municipal wastewaters using ceramic fine ultrafiltration membranes: Effect of feed solution pH and fouling phenomena. *Sep. Purif. Technol.* **2017**, *175*, 58–71. [CrossRef]
54. Rey, A.; Quiñones, D.H.; Álvarez, P.M.; Beltrán, F.J.; Plucinski, P.K. Simulated solar-light assisted photocatalytic ozonation of metoprolol over titania-coated magnetic activated carbon. *Appl. Catal. B Environ.* **2012**, *111–112*, 246–253. [CrossRef]
55. Rosa, S.M.C.; Nossol, A.B.S.; Nossol, E.; Zarbin, A.J.G.; Peralta-Zamora, P.G. Non-Synergistic UV-A Photocatalytic Degradation of Estrogens by Nano-TiO_2 Supported on Activated Carbon. *J. Braz. Chem. Soc.* **2016**, *28*, 582–588.
56. Ma, R.; Wang, X.; Huang, J.; Song, J.; Zhang, J.; Wang, X. Photocatalytic degradation of salicylic acid with magnetic activated carbon-supported F-N codoped TiO_2 under visible light. *Vacuum* **2017**, *141*, 157–165. [CrossRef]
57. Gar Alalm, M.; Tawfik, A.; Ookawara, S. Enhancement of photocatalytic activity of TiO_2 by immobilization on activated carbon for degradation of pharmaceuticals. *J. Environ. Chem. Eng.* **2016**, *4*, 1929–1937. [CrossRef]

58. Chen, Y.; Zhang, X.; Mao, L.; Yang, Z. Dependence of kinetics and pathway of acetaminophen photocatalytic degradation on irradiation photon energy and TiO_2 crystalline. *Chem. Eng. J.* **2017**, *330*, 1091–1099. [CrossRef]
59. Chang, C.T.; Wang, J.J.; Ouyang, T.; Zhang, Q.; Jing, Y.H. Photocatalytic degradation of acetaminophen in aqueous solutions by TiO_2/ZSM-5 zeolite with low energy irradiation. *Mater. Sci. Eng. B Solid-State Mater. Adv. Technol.* **2015**, *196*, 53–60. [CrossRef]